JP5.4   VALIDATION OF IMPROVED BROADBAND SHORTWAVE AND LONGWAVE FLUXES DERIVED FROM GOES

Mandana M. Khaiyer*, Michele L. Nordeen, Rabindra Palikonda, Yuhong Yi
Science Systems and Applications, Inc, Hampton, VA

Patrick Minnis and David R. Doelling
Atmospheric Sciences, NASA-Langley Research Center, Hampton, VA

1.   INTRODUCTION

Broadband (BB) shortwave (SW) and longwave (LW) fluxes at TOA (Top of Atmosphere) are a crucial parameter in the study of climate, and can be monitored over large portions of the Earth's surface using satellites. The VISST (Visible Infrared Solar Split-Window Technique) satellite retrieval algorithm facilitates derivation of these parameters from the Geostationery Operational Environmental Satellites (GOES). However, only narrowband (NB) fluxes are available from GOES, so this derivation requires use of narrowband-to-broadband (NB-BB) conversion coefficients. The accuracy of these coefficients affects the validity of the derived broadband (BB) fluxes. Previous studies documented NB-BB coefficients derived using broadband fluxes. These include 1986 ERBE-GOES6 comparisons (Minnis and Smith 1998), later updated with GOES8-TRMM comparisons (Chakrapani et al, 2003; Doelling et al, 2003). Most recently, NB-BB fits were re-derived using the NB fluxes from VISST/GOES data with BB fluxes observed by the CERES (Clouds and the Earth's Radiant Energy Budget) (Wielicki et al, 1998) instrument aboard *Terra*, a sun-synchronous polar-orbiting satellite that crosses the equator at 10:30 Local Time (Khaiyer et al, 2006).

Subsequent comparison with ARM's (Atmospheric Radiation Measurement) BBHRP (Broadband Heating Rate Profile) BB fluxes (Mlawer, personal communication) revealed that while the derived broadband fluxes agreed well with CERES near the *Terra* overpass times, the accuracy of both LW and SW fluxes decreased farther away from the overpass times. *Terra's* limited number of overpasses over a particular location on the Earth (twice daily) hampers the ability of the NB-BB fits to capture diurnal variability. To try to account for this in the LW, NB-BB fits are re-derived separately for day and night fits, as well as by season. Also, information from hourly SW BB fluxes provided from the Geostationery Earth Radiation Budget (GERB) instrument (Dewitte et al, 2008) aboard the Meteosat Second Generation (MSG) satellite is employed, to enhance the small solar zenith angle (SZA) range sampled by *Terra*. Validation of the BB fluxes derived from these improved NB-BB fits is performed using BB fluxes derived using Fu and Liou (2003) radiation code.

* *Corresponding Author Address*: Mandana M. Khaiyer, Science Systems and Applications, Inc., 1 Enterprise Parkway, Suite 200, Hampton, VA 23666; E-mail: m.m.khaiyer@nasa.gov

2. METHODOLOGY

VISST is used to process GOES-8 data with a nominal pixel resolution of 4 km. TOA NB fluxes from GOES can be derived from the VISST (Visible Infrared Solar Split-Window Technique; Minnis et al, 1995) satellite retrieval algorithm, which employs data from 0.65, 3.9, 11 and 12 um channels to retrieve cloud and radiative properties. NB albedoes can be derived in VISST from the 0.65 um radiance, and NB flux from the 11 um brightness temperatures. NB-BB coefficients are then employed to derive BB fluxes; these coefficients are derived by regressing GOES NB fluxes against BB fluxes observed by the CERES instrument aboard *Terra*.

The CERES BB SW and LW fluxes are provided per each footprint (20 km at nadir for Terra) by the Single Scanner Footprint TOA/Surface Fluxes and Clouds product (SSF). CERES further grids these SSF footprint data into a 1° gridded average product, the Monthly Gridded Surface Fluxes and Clouds (SFC). The CERES SFC fluxes (cross-track mode only) are compared to VISST/GOES 1° gridded NB fluxes within a 15 minute window, and for viewing zenith angles of less than 65° for CERES and 70° for VISST/GOES. To account for anisotropy within the radiance-to-flux conversion, CERES uses ADMs (Angular Distribution Models), which vary based on cloud and scene type (Loeb et al, 2003). CERES ADMs take into account 6 land scene types as well as a number of cloud variables including cloud fraction, phase, optical depth.

Using the comparisons of GOES NB to CERES BB fluxes, empirical equations can be used to convert NB flux to BB:

$$SWM_{bb} = a_0 + a_1*S_{nb} + a_2*S_{nb}{}^2 + a_3*\ln(1/csza)) \quad (1)$$

where SWM_{bb}= SW BB flux, S_{nb} = SW NB flux, csza=cos(SZA)

$$OLR_{bb} = A_0 + A_1*L_{nb} + A_2*L_{nb}{}^2 + A_3*L_{nb}*\ln(colRH) \quad (2)$$

where OLB_{bb} = LW BB flux, L_{nb}=LW NB flux, and colRH=column-weighted RH

VISST retrievals of GOES-8 data were made from March 2000 – February 2001, using Rapid Update Cycle (RUC) model results to provide vertical profiles of temperature and humidity. The VISST-derived NB and CERES-observed BB fluxes are used to derive coefficients for the Atmospheric Radiation Measurement (ARM) Program's Southern Great Plains (SGP) region, covering 32°N-42°N, 91°W-105°W. Four sets of seasonal coefficients for LW and SW NB-BB fits are derived employing the VISST and CERES data: spring

(Mar-May 2000), summer (Jun-Aug2000), fall (Sep-Nov 2000) and winter (Dec 2000-Feb 2001). To improve the diurnal variability in the LW NB-BB fits, separate fits are derived for daytime and nighttime. In order to enhance the SW NB-BB fits further by improving the SZA functionality, GERB enhancement is used.

To implement the GERB enhancement, SW NB-BB fits were created using 1° averaged MSG-1 NB versus GERB BB Edition 3 BARG (Binned Averaged Rectified Grid) fluxes from July 2006 and January 2007. Matching between these datasets is done over the region 39°N-45°N, 17°E-4°W, incorporating any 1° box with 99% or greater land amount in the matching. The SZA term (a3 from Eq. 3) from the GERB-MSG NB-BB fit is then employed in re-deriving new coefficients. To accomplish this, values of NB albedo are plugged into the a3 term from Eq. (1), and this resulting value is subtracted from the CERES BB flux; a0, a1, and a2 are then derived by re-regressing the narrowband values against the corrected CERES flux and a3 term. This helps account for some of the SZA range that *Terra*'s limited sampling cannot provide.

The BB fluxes derived in this way are then validated using the Fu-Liou radiation transfer model, a correlated-k, delta-two stream (2 for SW, 2/4 for LW) model. Spectral surface emissivity over 12 bands was provided by Wilber et al (1999). Inputs for the model were provided from different sources; the aerosol optical depths were derived from Multi-Filter Rotating Shadowband Radiometer (MFRSR), and surface albedo was derived from monthly mean CERES/SARB (Surface and Atmospheric Radiation Budget) maps. Sounding data was provided by European Center for Medium-Range Weather Forecasting/ Data Assimilation Office (ECMWF/DAO), and also provided skin temperature whenever VISST-derived skin temperature was unavailable.

3. RESULTS

Figure 1 shows a regression of VISST/GOES SW narrowband fluxes derived over the SGP (32°-42°N, 91°-105°W) versus *Terra* CERES BB fluxes from a) June-August 2000 (summer), and b) Dec00-Feb 2001 (winter). For 8,252 cases, the average summer CERES BB albedo is 0.2413, with an average VISST/GOES NB albedo of 0.2438; the regression RMS error is 6.9%. The winter cases yield an average CERES albedo of 0.3912, versus a VISST/GOES NB albedo of 0.4518. The regression coefficients (Ax) listed at plots' lower right can be used to convert narrowband fluxes to broadband, using equation (1) for SW. Regressions were also performed for spring and fall, but are not shown here.
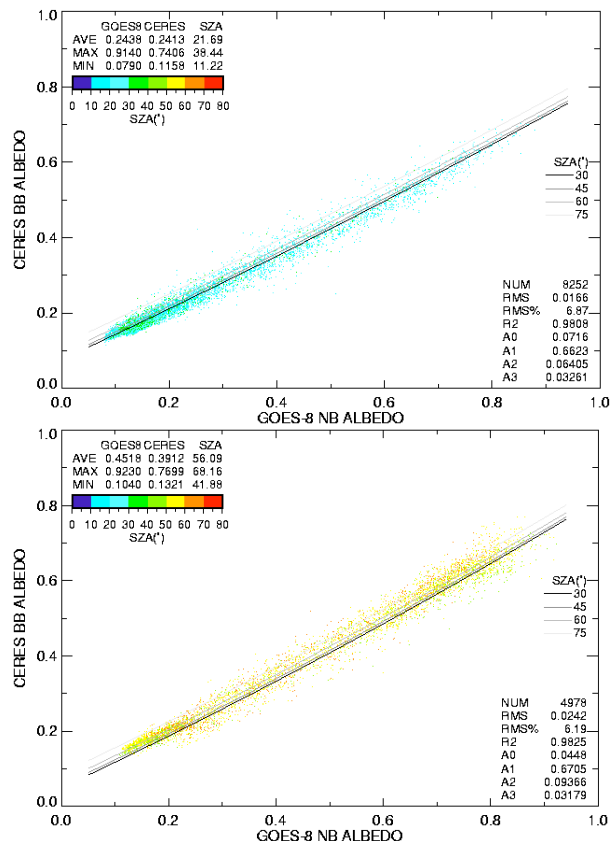

Fig.1 Regression of SW NB GOES and Terra CERES BB fluxes over the SGP (32°-42°N,91°-105°W), for a) summer (Jun-Aug00) and b) winter (Dec00-Feb01). The NB-BB coefficients (Ax) are listed at plots' lower right.

Using seasonal SW coefficients should yield good agreement at *Terra* overpass times, but the seasonal plots show a very limited range of SZA angle. In order to extend the SZA range to reflect what is likely to be observed throughout the day, GERB enhancement is used.

Figure 2 shows a side-by-side comparison of the VISST-derived BB fluxes compared with CERES BB, for the a) old operational 1 fit approach, and b) the improved seasonal fit approach. The new approach shows a decrease in bias from 1.1 W/m^2 down to 0.4 W/m^2, with a slight decrease in RMS error. This decrease proves that the improved SW NB-BB fits compare better at *Terra* overpass times. Due to *Terra*'s limited overpasses, these GOES-*Terra* NB-BB fits may not do well at capturing the diurnal variability, so outside enhancement is necessary to resolve the functionality with SZA. GERB's hourly observations of BB fluxes, compared to MSG's observations of NB fluxes at coincident times, can be used for this purpose.
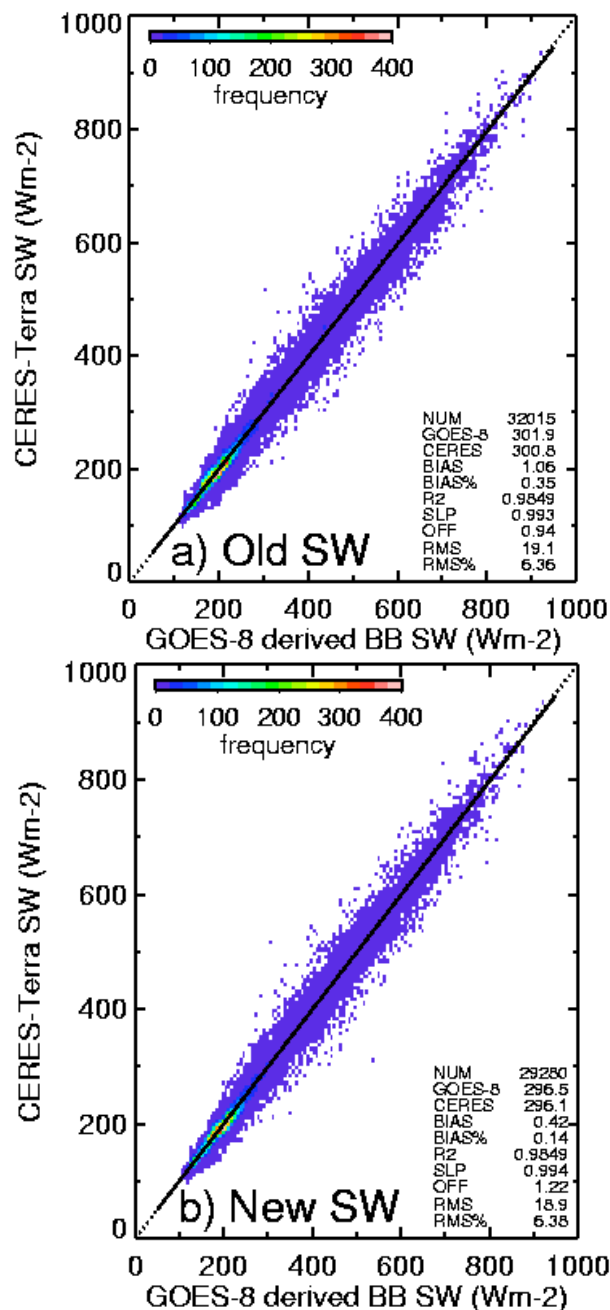
Fig.2 Validation of SW VISST-derived BB with CERES BB, for a) operational old fit and b) new seasonal fit approach.

Figure 3 shows the NB-BB regression fit for GERB-MSG for a) July 2006, b) January 2007. The higher SZA variability is apparent in these comparisons, due to the diurnal range of BB fluxes available to the geostationary MSG's GERB. The A3 term from the GERB-MSG fit is used in enhancing the SGP SW NB-BB fits. For Jul06, the term is 0.04856, and for Jan07 it is 0.03438. These terms are employed in the SGP SW NB-BB fits to improve accuracy of VISST-derived GOES BB fluxes at times beyond the *Terra* overpasses; the Jul06 A3 term
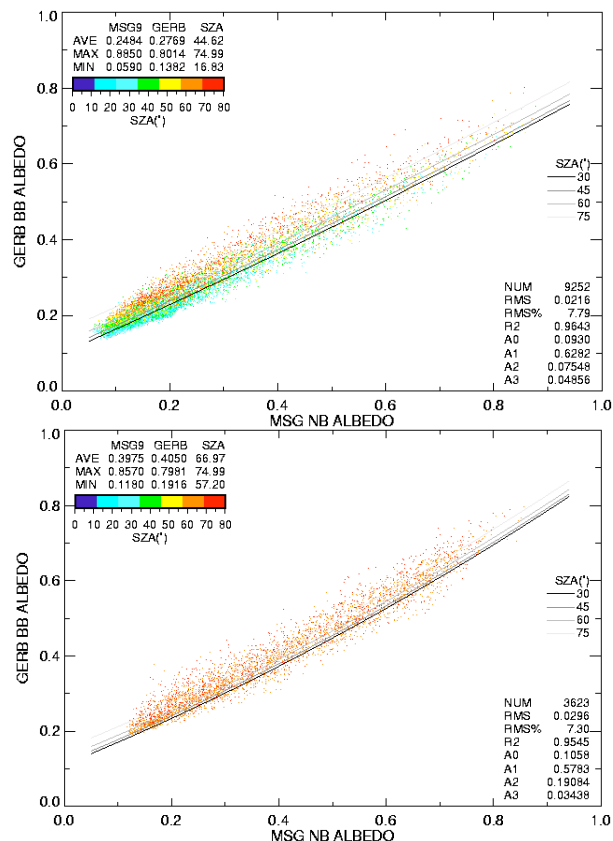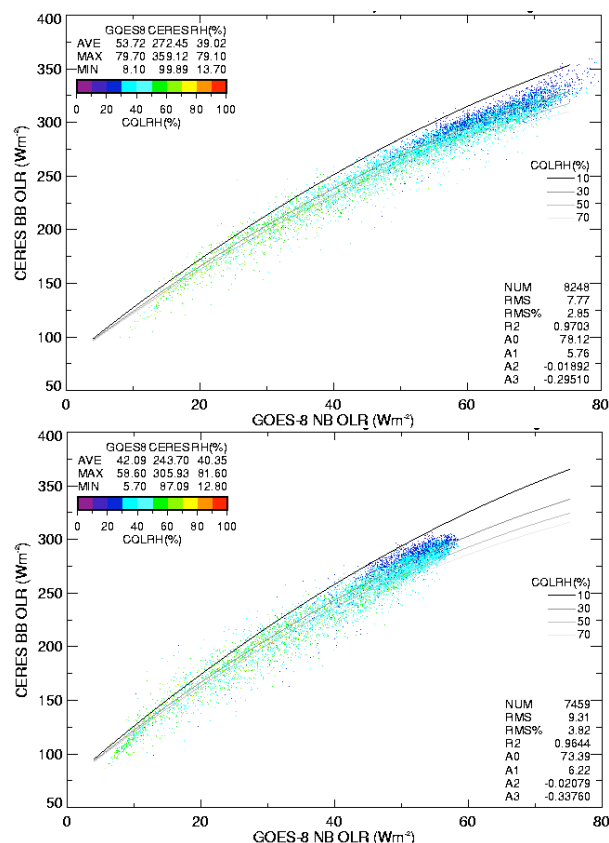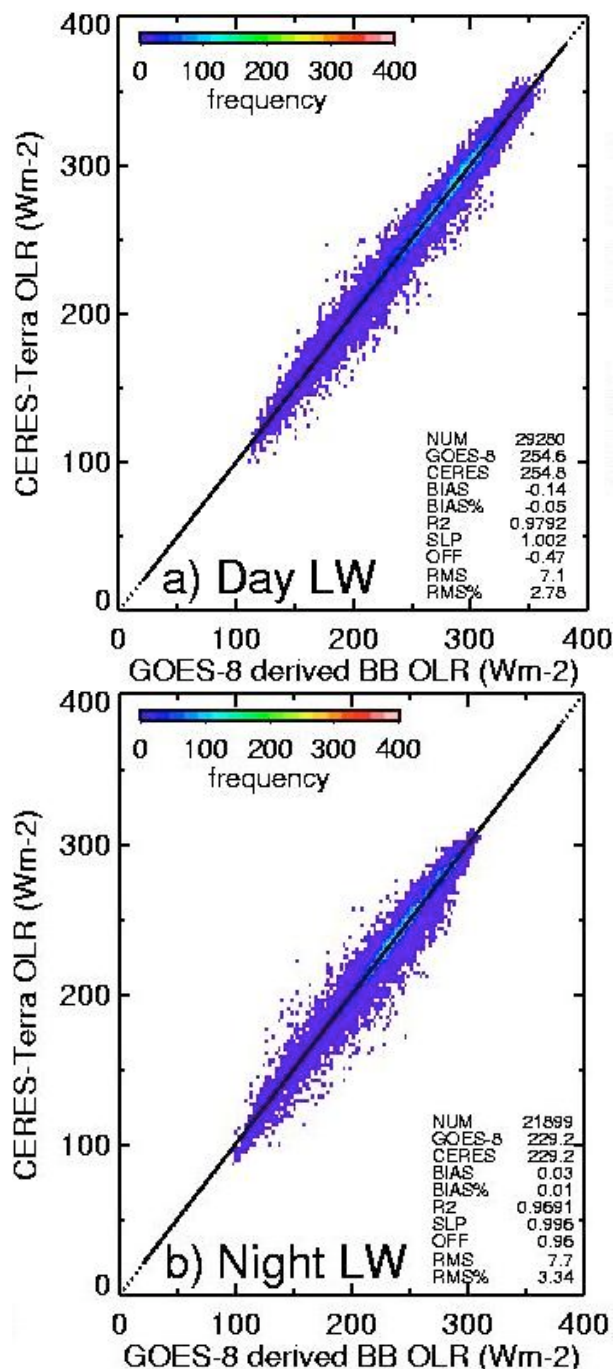

Fig.3 Regression of SW NB MSG and GERB BB fluxes over land in Europe (39°-45°N,4°E-17°W), for a) summer (Jul06) and b) winter (Jan07). The NB-BB coefficients (Ax) are listed at plots' lower right.

is used in the summer fit, and the Jan07 term in all other seasonal fits.

The SGP LW NB-BB fit is also improved to capture diurnal variability beyond the fits derived in earlier studies, by deriving separate fits for daytime and nighttime. Figure 4 shows summertime NB-BB regression fits for the LW over the SGP. For 8248 cases, the average daytime CERES BB LW flux is 272.5 W/m^2, corresponding to an average VISST/GOES NB flux of 53.7 W/m^2. The RMS error is 2.9%. For nighttime, CERES BB flux decreases to an average of 243.7 W/m^2 and GOES NB flux decreases to 42.1 W/m^2. As with the SW, regressions were also performed for winter, spring and fall, but are not shown here. The regression coefficients (Ax) listed at plots' lower right can be used to convert NB fluxes to BB, using equation (2) for LW. A third order correction is added to the data to eliminate low-end bias.

Fig.4 Regression of LW NB GOES and Terra CERES BB fluxes over the SGP (32°-42°N,91°-105°W), for Summer (Jun-Aug00) a) Daytime cases and b) Nighttime cases. The NB-BB coefficients (Ax) are listed at plots' lower right.

The implementation of separate LW NB-BB fits for day and night leads to a marked improvement in the day-night bias. With the operational 1-fit approach, the daytime bias was 0.8 W/m^2 (RMS 7.4 W/m^2) and the nighttime was -4.7 W/m^2 (RMS 7.7 W/m^2) (not shown). The improved seasonal/day/night fits lead to a decreased daytime bias of -0.1 W/m^2 (RMS 7.1 W/m^2) and a nighttime bias of 0.0 W/m^2 (RMS 7.7 W/m^2) (see Fig. 5).

.

Fig.5 Comparison of LW CERES BB fluxes (y-axis) and GOES BB fluxes (x-axis) derived using updated seasonal/day/night NB-BB fits for a) daytime and b) nighttime.

4. DISCUSSION

Comparisons have been made of the seasonal VISST-derived BB fluxes with CERES observed BB fluxes, which show the updated fits agree well at Terra overpass times. However, this is a very limited validation. In order to fully gauge the effects of these new fits on the derivation of BB fluxes, validation must
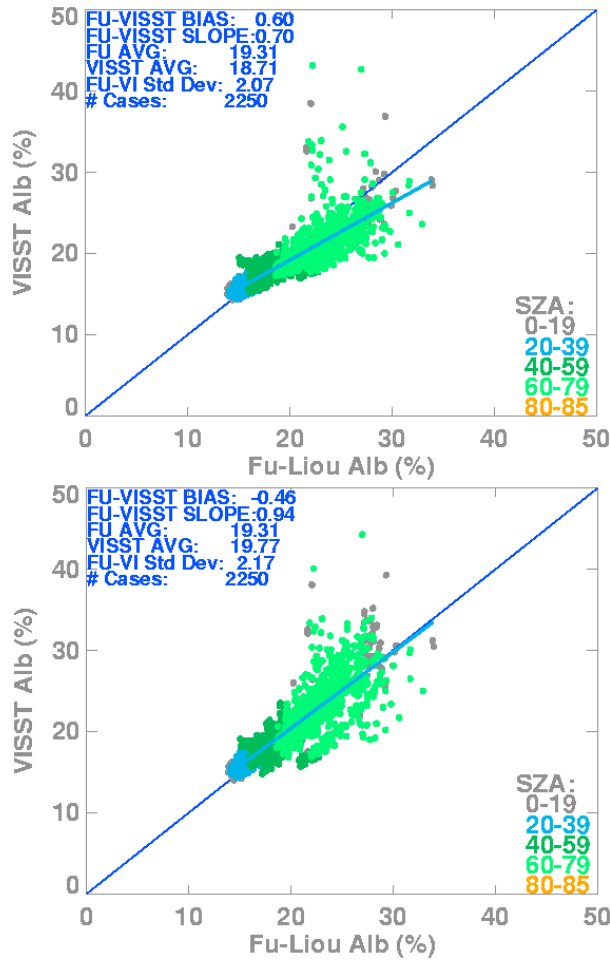
Fig.6 Comparison of clear-sky Fu-Liou-derived SW BB albedoes (x-axis) with VISST-derived (y-axis) a) operational fit, b) updated seasonal GERB-enhanced fit.

Fig. 7 Diurnal plot of half-hourly averaged BB SW albedoes for Fu-Liou (blue), VISST operational fit (red), and seasonal GERB-enhanced fit (green).

Compared to Fu-Liou, the GERB-enhanced seasonal VISST fits yield a more realistic diurnal cycle than the operational fits. However, the BB albedoes derived from the updated fit diverge from Fu-Liou-derived albedoes closer to sunrise and sunset. The magnitude of the GERB SZA term will affect the amplitude of the albedoes' diurnal curve. Therefore factors affecting the SZA term must be examined; issues such as differences in the terrain of Europe, versus that of the SGP, may affect the GERB-MSG SZA terms.

be made with data from throughout the diurnal cycle. Fu-Liou derived BB fluxes are employed to facilitate this validation.

Figure 6 shows a scatterplot of clear-sky VISST-derived BB SW fluxes (y-axis) versus Fu-Liou (x-axis) derived from a) operational 1 fit data, and b) seasonal, GERB-enhanced new fits. The data is color-coded by SZA, and is limited to SZA< 80°. Although the bias is only 0.6%, the operational 1 fit data shows a marked departure from the one-to-one agreement line, with a slope of 0.70. However, employing the new seasonal GERB-enhanced fits leads to a slightly smaller bias as well as a slope of 0.94, showing better agreement. A scatterplot of all cases (clear and cloudy; not shown) shows that the bias decreases from 1.1% to 0.04% with use of the updated fits, and the slope improved slightly from 0.89 to 0.90.

To examine errors in the VISST-derived BB SW albedoes with time, half-hour averages are compared with Fu-Liou throughout the day (Fig. 7). The red curve shows the diurnal curve of SW BB albedoes derived from the operational VISST fit, the blue shows the Fu-Liou-derived albedoes, and the green shows the improved GERB-enhanced VISST-derived albedoes.
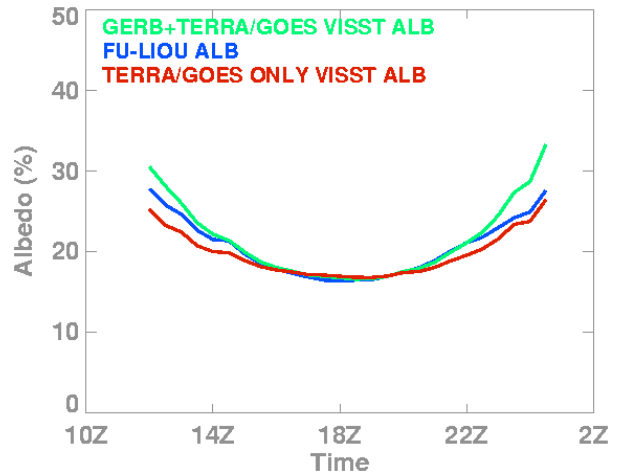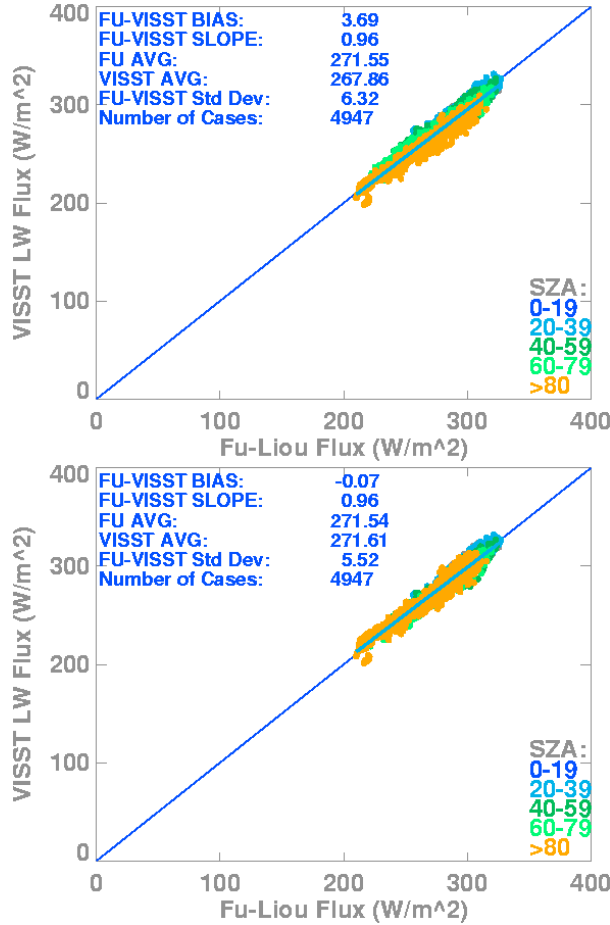
Fig.8 Comparison of clear-sky LW Fu-Liou-derived BB albedoes (x-axis) versus VISST-derived (y-axis) for a) operational fit, and b) updated seasonal/ day/night fit.

The updated seasonal/day/night LW fits are also evaluated with respect to Fu-Liou. Figure 8 shows the clear-sky comparison of a) operational VISST-derived BB LW fluxes and b) seasonal/day/night VISST-derived BB LW versus Fu-Liou. The comparison between Fu-Liou and the operational VISST shows a bias of 3.7 W/m^2 that decreases to -0.1W/m^2 when the updated LW fits are employed. The slope is the same (0.96) for both the operational and updated fits. For all cases (clear and cloudy; not shown) the bias of 0.2 W/m^2 is closer to 0 for the operational fit; the magnitude of the bias increased to -2.1 W/m^2 for the updated fit. Even so, the updated NB-BB fit yielded VISST BB fluxes that had a better slope of agreement (0.93, vs. 0.91 for the old fit).

To examine the errors throughout the day, the VISST-derived BB LW fluxes are averaged by half-hour and plotted in Fig. 9 for a) clear-sky cases and b) all cases. For the clear-sky cases, the seasonal/day/night fit-derived fluxes track Fu-Liou more closely during nighttime than the operational NB-BB fit. Both the operational and updated NB-BB fits track Fu-Liou well during the day, until the afternoon when they underpredict Fu-Liou. This phenomena could be due to a terrain-related azimuthal effect. The diurnal curves for total cases show that fluxes derived from the updated

NB-BB fits overpredict Fu-Liou considerably at night, while the operational fit underpredicts slightly. Both fits overpredict slightly in the morning.
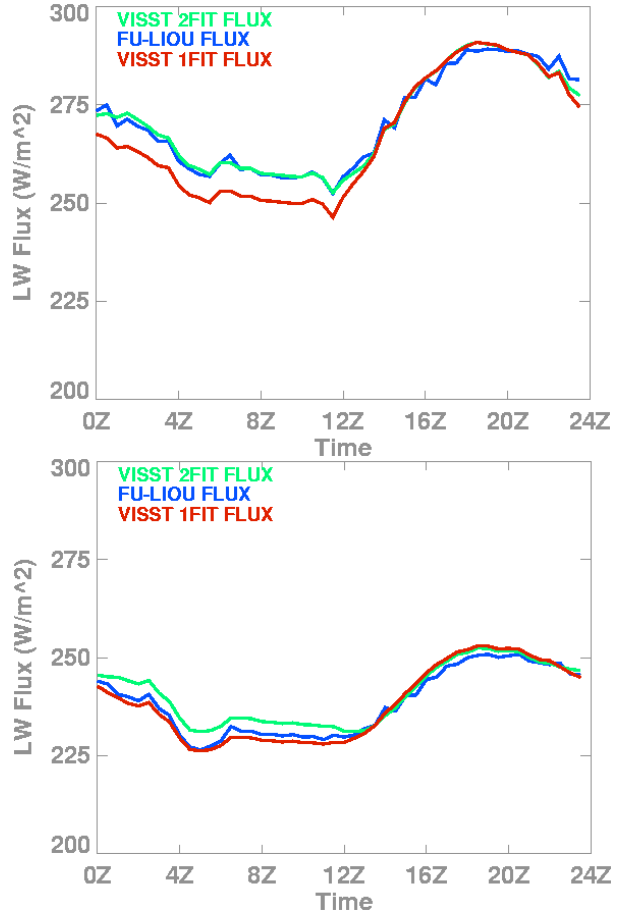

Fig. 9 Diurnal plot of half-hourly averaged BB LW fluxes for Fu-Liou (blue), VISST operational fit (red), and seasonal GERB-enhanced fit (green), for a) clear-sky cases, and b) total (clear and cloudy) cases.

5. SUMMARY AND FUTURE WORK

The updated LW and SW NB-BB fits show promise in improving the accuracy of VISST-derived BB fluxes. For the SW NB-BB fit, the GERB enhancement yields a more realistic diurnal cycle than the operational SW NB-BB fit. Discrepancies with Fu-Liou closer to sunrise and sunset may be due to differences in terrain affecting the GERB-MSG SZA term; the terrain MSG observes in Europe is different from that over the SGP viewed by GOES. Overall, the seasonal derivation and GERB enhancement seem to improve the SW NB-BB fit.

For the LW, the diurnal curves show that there is a discrepancy between clear and total cases with the operational and updated VISST-derived fluxes, and this must be resolved. However, most indicators are that the day/night/seasonal LW NB-BB fits improve the derivation of BB LW fluxes. As future work, the SGP LW NB-BB fits will be evaluated with GERB-MSG LW NB-BB fits.

Additionally, improvement of the SW NB-BB fits will include implementation of the A3 terms from 4 selected months of GERB-MSG NB-BB (Jul06, Oct06, Jan07, Apr07), applied to each corresponding season; this should account for both the green-up and brown-down phases of SGP SW NB-BB fits. Once the improvement in NB-BB fits is complete, the fits will also be re-derived for other domains (e.g. Tropical Western Pacific, Pt. Reyes) using these updated techniques.

6. ACKNOWLEDGEMENTS

7. REFERENCES

Chakrapani, V., D. R. Doelling, A. D. Rapp, and P. Minnis, 2002: Cloud thickness estimation from GOES-8 satellite data over the ARM SGP site. *Proc. 12th ARM Science Team Meeting*, April 8-12, St. Petersburg, FL, 14 pp. Available at http:// www.arm.gov/docs/documents/technical/conf_0204/ chakrapani-v.pdf.

Geier, E.B., R. N. Green, D. P. Kratz, P. Minnis, W. F.Miller, S. K. Nolan, and C. B. Franklin, 2001: Single satellite footprint TOA/surface fluxes and clouds (SSF) collection document. [available on-line from http://asd-www.larc.nasa.gov/CERES ASDceres.html.]

Dewitte, S., L. Gonzalez, N. Clerbaux, A. Ipe, C. Bertrand, B. De Paepe, 2008: The Geostationary Earth Radiation Budget Edition 1 data processing algorithms, *Advances in Space Research*, Vol. 41, No. 11, 1906-1913, doi:10.1016/j.asr.2007.07.042

Doelling, D. R., M. M. Khaiyer, and P. Minnis, 2003: ARM-SGP TOA OLR Fluxes from GOES-8 IR Radiances Based on CERES Data. *Proc. 13th ARM Science Team Meeting*, March 31-April 4, Broomfield, CO, 10 pp. Available at http://www.arm.gov/publications/proceedings/conf13/ extended_abs/doelling-dr.pdf

Fu, Q. and K. N. Liou, 1993: Parameterization of the radiative properties of cirrus clouds. *Journal of Atmospheric Sciences*, **50**, pp. 2008-2025

Khaiyer, M. M., D. R.Doelling, P. K. Chan, M. L. Nordeen, R. Palikonda, Y. Yi, D. N. Phan, and P. Minnis, 2006: Derivation of Improved Surface and Top of Atmosphere Broadband Shortwave and Longwave Fluxes over Atmospheric Radiation Measurement Program Domains. *Proc. 16th ARM Science Team Meeting*, March 27-31, Albuquerque, NM, 13 pp. Available at http://www.arm.gov/publications/proceedings/conf16/ extended_abs/khaiyer_mm.pdf

Loeb, N.G., N.M. Smith, S. Kato, W.F. Miller, S.K.Gupta,

P. Minnis, and B. A. Wielicki, 2003: Angular distribution models for top-of-atmosphere radiative flux estimation from the Clouds and the Earth's Radiant Energy System instrument on the Tropical Rainfall Measuring Mission Satellite. Part I: Methodology, J.Appl. Meteor., 42, 240-265

Minnis, P. and Smith, W. L., Jr., 1998: Cloud and Radiative Fields Derived from GOES-8 During SUCCESS and the ARM-UAV Spring 1996 Flight Series. *Geophys. Res. Ltrs.,* 25, pp.1113-1116.

Minnis, P., D. P. Kratz, J. A. Coakley, Jr., M. D. King, D. Garber, P. Heck, S. Mayor, D. F. Young, and R. Arduini, 1995: Cloud Optical Property Retrieval (Subsystem 4.3). "Clouds and the Earth's Radiant Energy System (CERES) Algorithm Theoretical Basis Document, Volume III: Cloud Analyses and Radiance Inversions (Subsystem 4)", NASA RP 1376 Vol. 3, edited by CERES Science Team, pp. 135-176.

Wielicki, B. A., et al., 1998: Clouds and the Earth's Radiant Energy System (CERES): Algorithm Overview. *IEEE Trans. Geosci. and Remote Sens*., 36, 1127-1141.

Wilbur, A.C., D.P.Kratz, S.K.Gupta, 1999: Surface Emissivity Maps for Use in Satellite Retrievals of Longwave Radiation. NASA/TP-1999-209362, 35 pp.